Factors That Determine the Performance of Carbon Fuels in the Direct Carbon Fuel Cell

ARTICLE *in* INDUSTRIAL & ENGINEERING CHEMISTRY RESEARCH · DECEMBER 2008

Impact Factor: 2.59 · DOI: 10.1021/ie800891m · Source: OAI

7 AUTHORS, INCLUDING:

Andrew Dicks
LC Energy
63 PUBLICATIONS **3,658** CITATIONS
SEE PROFILE

Shaomin Liu
Curtin University
221 PUBLICATIONS **4,932** CITATIONS
SEE PROFILE

Factors That Determine the Performance of Carbon Fuels in the Direct Carbon Fuel Cell

Xiang Li,[†] Zhong Hua Zhu,*[,†] Roland De Marco,[‡] Andrew Dicks,[†] John Bradley,[†] Shaomin Liu,[†] and Gao Qing Lu[†]

Division of Chemical Engineering and ARC Centre for Functional Nanomaterials, University of Queensland, Brisbane 4072 QLD, Australia, and Department of Applied Chemistry, Curtin University of Technology, Perth, Australia

The direct carbon fuel cell (DCFC) is a promising power generation device, which has a much higher efficiency (80%) and a lower emission than conventional coal-fired power plants. In this study, different commercial carbon fuels including activated carbon (AC), carbon black (CB220 and CB660), and graphitic carbon (GC) were tested in DCFC at 600−800 °C. The relationship between the intrinsic properties of carbon fuels and their electrochemical performance in the DCFC was analyzed. It is found that a desirable carbon fuel for DCFC should have high mesoporous surface area and rich oxygen-containing surface groups. The anodic performance of the DCFC may also be improved by small carbon particle size, fast stirring rates, and high cell temperatures.

1. Introduction

The need for clean energy production coupled with increased energy demand poses one of the greatest challenges in the 21st century, and fuel cell technology is one of the most effective solutions for the impending energy crisis. The direct carbon fuel cell (DCFC), a novel high-temperature fuel cell, is drawing ever-increasing attention due to its high conversion efficiency with low pollution. Differing from other fuel cells, the DCFC is the only fuel cell type converting solid carbon into electricity without an intermediate reforming process. The solid carbon fuels for the DCFC can be easily produced from various resources, including coal, petroleum, natural gas, and even biomass. Particularly, coal is the most abundant fossil resource on the earth and accounts for 60% of the world's fossil fuel consumption, but most energy reserves of coal remain underused.[1−3] The DCFC technology provides a promising opportunity to improve the utilization of fossil fuel and reduce air pollution. Compared with other fuel cells powered by hydrogen, the DCFC has the thermodynamic advantage of a near-zero entropy change at high temperature, which means the theoretical electrochemical efficiency of the DCFC ($\Delta G/\Delta H$) is almost 100%.[1−7] Even under practical operating conditions, ~80% efficiency can be reached in the DCFC system. Moreover, the activities (chemical potentials) of both reactant carbon and the product carbon dioxide are fixed, resulting in a stable carbon anode potential during practical operation.[2,3] Finally, the DCFC has lower emissions compared with conventional power plants. In principle, the off gas is almost pure carbon dioxide which can be directly collected for industrial use or sequestration. If coal is used as the fuel for the DCFC, carbon emissions could be reduced by 50%, and the off gas may be reduced by 10 times than that of coal-fired power plants.[1]

Until now, there have been different attempts to convert carbon materials directly into electricity in the DCFC with various electrolytes, such as molten carbonates,[2,3,8−13] molten hydroxides,[7,14−17] and YSZ-based solid electrolytes.[18,19] However, the most attractive approach for the DCFC is using mixed molten carbonate electrolytes (e.g., $Li_2CO_3-Na_2CO_2-K_2CO_3$) as the carbon oxidation medium. This is because the mixed molten carbonates have high stability and electrical conductivity, low volatility and toxicity, and relatively low melting points. The latest development in the DCFC is to utilize highly reactive carbon particulates dispersed in the molten electrolyte, between an anode and a cathode at high temperature.[2,3,9,11,12] The anode and cathode reactions in this system may be expressed by eqs 1 and 2, and the overall reaction is given by eq 3.

$$\text{anode reaction:} \quad C + 2CO_3^{2-} \rightarrow 3CO_2 + 4e^- \tag{1}$$

$$\text{cathode reaction:} \quad O_2 + 2CO_2 + 4e^- \rightarrow 2CO_3^{2-} \tag{2}$$

$$\text{overall reaction:} \quad C + O_2 \rightarrow CO_2 \tag{3}$$

where the anode potential is given by eq 4:

$$E = E^\circ - (RT/4F)\ln[P_{CO_2}{}^3(w)] + (RT/4F)\ln[P_{CO_2}{}^2(r)P_{O_2}(r)] \tag{4}$$

where E° is the anode potential at standard condition, R is the universal gas constant, and T is the cell temperature (K). $P_{CO_2}(w)$ is the ratio of CO_2 partial pressure to total pressure at working electrode, while $P_{CO_2}(r)$ and $P_{O_2}(r)$ are the ratios of partial pressures of CO_2 and O_2 to total pressure at the reference electrode.

Although various carbon fuels have been tested in different DCFC apparatus, a knowledge of the efficacy of carbon fuels is still unclear. It is apparent that the disordered carbon is more reactive due to a preponderance of edges sites and defects, but graphitic carbon with high electrical conductivity may also benefit the electrochemical reactivity. The physical and chemical properties of carbon fuels can be seen to highly influence the electrochemical performance. Weaver et al. found that carbon fuels with high surface areas, such as devolatilized coal, are more accessible to the anode reaction.[13] However, Cooper's group concluded that the effect of carbon's surface area alone on the discharge rate is relatively weak.[2,3] Accordingly, there is a need to develop approaches to improve the electrochemical reactivity of carbon fuels in the anode reaction (1).

* Corresponding author. Fax: 61 7 3365 4199. E-mail: address: z.zhu@uq.edu.au.
[†] University of Queensland.
[‡] Curtin University of Technology.

10.1021/ie800891m CCC: $40.75
Published on Web 11/07/2008

In this paper, four commercial carbon fuels (one activated carbon, two carbon blacks, and one graphitic carbon) were characterized and tested in our DCFC system. The structural properties and reactivities of carbon fuels were compared. Particularly, the relationship between carbon fuel surface complex and the concomitant electrochemical performance of the DCFC was investigated. In order to improve the anodic performance of the DCFC, we also studied the effects of operating conditions (such as carbon loading and particle size, stirring rate, and cell temperature) on the performance of the DCFC.

2. Experimental Section

2.1. Characterization of Carbon Fuels. Four commercial carbons were selected to cover a wide range of carbon reactivities. The granular activated carbon (Calgon BPL, 4ΔA6 mm) was ground and sieved into four different particle sizes ranges: smaller than 0.07 mm, 0.07−0.25 mm, 0.25−0.45 mm, and 0.45−1.5 mm, which were designated as AC-S, AC-M, AC, and AC-L, respectively. Two of the carbon blacks (Koppers Continex N220 and N660) with 0.1−0.2 mm particle size were designated as CB220 and CB660. The graphitic carbon (TIMCAL M-292) with particle size of 0.1−0.2 mm was designated as GC.

XRD patterns of the four carbon samples were performed on a Rigaku Miniflex X-ray diffractometer (40 kV, 30 mA) with Cu Kα radiation at a scanning rate of 2°/min in the 2θ range from 10° to 90°. The average size of carbon crystalline was calculated from the Debye−Scherer equation:

$$L = \frac{K\lambda}{\beta \cos \theta} \tag{5}$$

where λ is the wavelength of the X-rays, θ is the diffraction angle, K is the shape factor, and β is the peak width at half-maximum intensity. The values of $K = 0.9$ and 1.84 were used for L_c and L_a determination, respectively. L_c, the layer dimension perpendicular to the basal plane, is obtained from the (002) reflection. L_a, the layer dimension parallel to the basal plane, is calculated by the (100) reflection.

Electrical conductivities were measured by a frequency response analyzer (Solartron SI1260). First, ∼200 mg of carbon material was pressed into a small pellet (13 mm diameter) at 150 kg/cm^2. This sample pellet was placed between two gold-plated blocking electrodes of 0.5 cm^2 area in a chamber, and the impedance of the sample was measured over a frequency range 1 MHz to 1 Hz at an amplitude of ±10 mV root mean square (rms). Finally, the bulk conductivity σ (S/cm) could be calculated from the equation

$$\sigma = l/[(r - r_0)A] \tag{6}$$

where l is the sample pellet thickness(cm), r is the tested sample resistance (taken as the impedance at zero phase angle, Ω), r_0 is the rig short-circuit resistance (Ω), and A *is* the electrode contact area (0.5 cm^2).

N_2 adsorption experiments were carried out in a NOVA-1200 adsorption analyzer (Quantachrome) at 77 K. All carbon fuel samples were degassed at 200 °C for 8 h prior to the N_2 adsorption measurement. The specific surface areas (S_{BET}) of the carbon samples were calculated by the multiple point Brunauer−Emmett−Teller (BET) method. The total pore volume (V_{total}) is derived from the adsorption amount at a relative pressure of $P/P_0 = 0.99$. The micropore surface areas (S_{micro}) of all carbons were calculated by the available software (QuadraWin V2.0) which applies the density functional theory (DFT) method. The mesoporous surface area is obtained as the difference between the total surface area and the microporous surface area.

Temperature-programmed oxidation (TPO) measurements were investigated under air flow (80 mL/min) in a thermogravimetric analyzer (Shimadzu TGA-50). Samples were loaded into a platinum pan and heated under a nitrogen atmosphere from room temperature to 200 °C and held for 1 h to remove the adsorbed water, and then the temperature was further increased to 900 °C in air (80 mL/min) at a heating rate of 10 °C/min.

The X-ray photoelectron spectroscopy (XPS) measurements were conducted using a Kratos Axis Ultra XPS system incorporating a 165 mm hemispherical electron energy analyzer. The incident radiation was monochromatic Al Kα X-ray (1486.6 eV) at 150 W (15 kV, 10 mA). Survey scans were taken at an analyzer pass energy of 160 eV and carried out over 1200 eV binding energy range with 1.0 eV and a dwell time of 100 ms.

The mass titration method of Noh and Schwarz[20] was used to estimate the point of zero charge (PZC) on the carbon surfaces. Three initial pH solutions (pH 3, 6, 11) were prepared using HNO_3 (0.1 M) and NaOH (0.1 M). Sodium nitrate was used as the background electrolyte. For each initial pH, six containers were filled with 20 mL of the solution, and different amounts of carbon were added (0.05, 0.10, 0.50, 1.00, and 10 wt %). The equilibrium pH was measured after 24 h. The plot of pH vs mass fraction showed a plateau, and the PZC was then identified as the point at which the change in pH was negligible. The PZC was then taken as the average of the three asymptotic pH values.

Temperature-programmed desorption (TPD) experiments were carried out in a vertical tube furnace with Ar (80 mL/min) as the carrier gas. A 0.5 g sample was placed in a quartz tube, heated to 110 °C for 60 min and then at 5 °C/min to 900 °C. The gases evolved were analyzed using a chromatograph (Shimadzu GC-17A) equipped with a thermal conductivity detector and a Carbosphere column.

2.2. Evaluation of Carbon Fuels in DCFC. A schematic diagram of our DCFC is shown in Figure 1, which is similar to the approach of Vutetakis et al.[11,12] The working electrode (WE) typically consists of a solid gold rod (serve as a current collector, 99.9% purity and 3.2 mm diameter) that was cemented to the end of an alumina tube (7 mm diameter). A gold wire was spot-welded to the gold rod and extended to the other end of the alumina tube for connecting to the potentiostat. The total exposed surface area of the gold rod was 3.0 cm^2. The counter electrode (CE) was made from a gold sheet (with 1.0 cm^2 surface area) spot-welded to a gold wire, and the gold parts were sheathed in a closed-bottom alumina tube (12 mm diameter). A 1.5 mm hole at the bottom of the alumina sheath allowed contact of the electrolytes between the CE and the WE. The reference electrode (RE) was constructed from an alumina sheath (12 mm diameter) containing a gold wire in contact with the electrolyte melts, and a 0.05−0.1 mm pinhole (by the laser drill) at the bottom of the alumina sheath offered the contact of electrolyte between the RE and WE. The particulate carbon fuels with the ternary molten carbonate electrolyte (32% Li−34% Na−34% K eutectic) were contained in a large alumina crucible. In order to keep the entire cell in a gastight environment, the alumina crucible was placed at the bottom of an inconel canister and sealed by a water-cooled brass lid. The three electrodes and gas feed tubes were supported by the brass lid and inserted into the WE anode compartment. An inconel stirring rod with

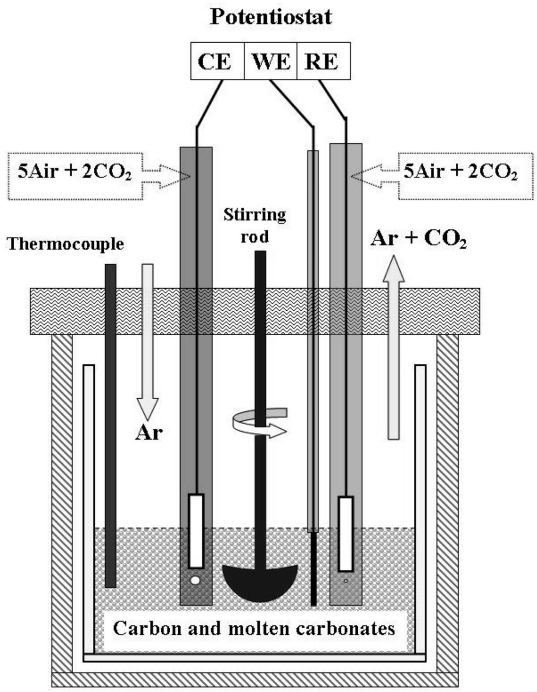

Figure 1. Schematic diagram of direct carbon fuel cell.

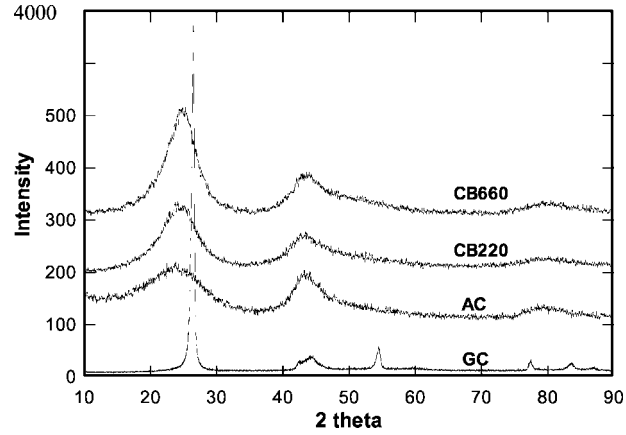

Figure 2. XRD patterns of AC, CB660, CB220, and GC.

Table 1. Crystalline Parameters, Electrical Conductivities, and Pore Structures of AC, CB660, CB220, and GC

carbon fuels	XRD			electrical conductivity σ (S/cm)
	d_{002} (nm)	L_c (nm)	L_a (nm)	
AC	0.373	1.0	4.5	0.8
CB660	0.363	1.7	3.5	1.8
CB220	0.368	1.5	2.9	1.5
GC	0.336	18.3	9.4	10.5

a half-circle impeller (3 cm diameter) and a type K thermocouple were also placed in the molten carbonate electrolyte.

Prior to each experiment, dry 250 g ternary carbonate powders were mixed with the carbon fuels to a certain concentration (typically 1, 5, and 10 wt % carbon). The gold parts of the three different electrodes were washed by nitrohydrochloric acid for 10 s and rinsed with distilled water followed by acetone. After the fuel cell was assembled and sealed gastight, it was heated by a crucible furnace (Lindberg Blue/M) at a heating rate of 3 °C/min. During the heat-up, Ar (150 mL/min) was purged into the WE compartment and CO_2 (50 mL/min) was purged into the CE and RE compartments. Once the required operating temperature was reached, the Ar and CO_2 purge rates were decreased to 70 and 15 mL/min, respectively. At the same time, air (35 mL/min) was introduced into the CE and RE compartments. Finally, the carbon anode half-cell measurements were performed with a potentiostat (Autolab PGSTAT302), using the GPES and FRA software package (Version 4.9). For the linear sweep voltammetry measurements, the anodic polarization (relative to reference electrode) started from the open-circuit voltage (OCV) to the 0.0 V (relative to RE) at scan rate of 1 mV/s. Note that under open-circuit conditions the potential of the reference electrode is the same as the cathode, and therefore the potential difference between the anode and reference is taken as the OCV.

In order to obtain an estimate of power produced by the DCFC at a given current density, the anode potential (WE relative to RE) is multiplied by the corresponding current density to calculate the theoretical power density. Here we focus on the maximum theoretical power density (P_{max}), i.e., the maximum value of the theoretical power density for a certain anode potential versus current density curve (or $V-i$ curve). It should be pointed out that the real fuel cell power density is determined by the cell voltage (i.e., the potential difference between anode and cathode) and not just the anode potential. Since the reactivity of the anode was the main focus of this work, the cathode potential was not measured, and cell voltages are therefore not reported. For the $V-i$ curves collected in different stirring conditions, the linear sweep procedure was repeated as soon as a stable OCV was reached again. However, for the polarization data collected at different carbon loading conditions, the whole experimental procedure was repeated from drying of new carbonates to the final electrochemical measurements.

3. Results

3.1. Graphitic Structures of Carbon Fuels. XRD patterns of four different carbon fuels are shown in Figure 2. For GC, an intense peak corresponding to the (002) graphitic basal plane reflection can be observed at 26.5°, and many other differentiable peaks at high 2θ values reveal the highly ordered crystalline structure. For CB660, CB220, and AC, a broad diffraction peak can be observed at about $2\theta = 24°$ in each pattern, which is attributed to the (002) reflection. Another weak broaden peak at around 44° is attributed to the equivalent (100) graphite crystal faces reflection. Only the asymmetric (002) and (100) peaks maxima are characteristic of a turbostratic crystalline structure for carbon. The (002) and (100) peaks of these three carbon materials shift to relatively lower values than those of GC, which also indicates that CB660, CB220, and AC have a more disordered structure than GC.

The quantitative crystalline parameters of all carbon fuels including interplanar distance (d_{002}), the average diameter (L_a), and the stacking height (L_c) are shown in columns 2−4 of Table 1. As expected, the GC has the smallest d_{002} and largest L_a and L_c values due to its highest degree of graphitic structure. CB660, CB220, and AC show similar d_{002} values at the range of 0.36−0.37 nm, which are higher than that of GC. However, the L_a and L_c values of the three carbon fuels are much smaller than that of GC. These data further confirm that CB660, CB220, and AC have more disordered crystalline structure than GC.

3.2. Electrical Conductivity of Carbon Fuels. Electrical conductivity of the carbon fuel is known to be critical for the performance of the DCFC, since carbon fuels will not only be consumed by the electrochemical reaction but also are contacted by the current collector directly assisting with the transfer of electrons.[2] It is well-known that electrical conductivity is highly

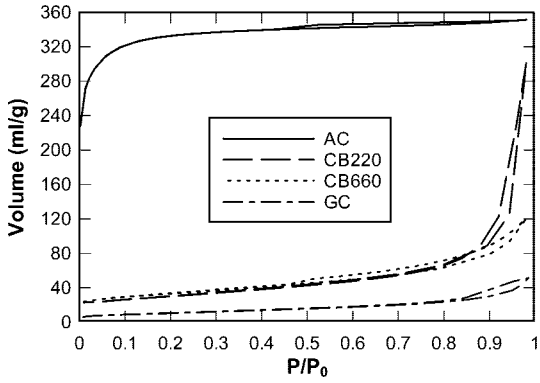

Figure 3. N_2 adsorption isotherms of AC, CB660, CB220, and GC.

Table 2. Pore Structure of All Carbon Fuels

sample	S_{BET} (m^2/g)	V_{total} (cm^3/g)	S_{micro} (m^2/g)	S_{meso} (m^2/g)
CB220	118	0.28	35	85
CB660	106	0.19	28	78
GC	39	0.08	5	34
AC	1241	0.55	1110	131
AC-L	1212	0.55	1118	84
AC-M	1268	0.56	1087	181
AC-S	1305	0.58	1091	214

dependent on the degree of graphitic structure. Usually, a more ordered carbon has a higher electrical conductivity. The bulk conductivity values of all carbon fuels are listed in the column 5 of Table 1. As expected, the GC has the highest conductivity (10.5 S/cm) because of its highest degree of graphitic structure in all of the carbons. In contrast, the AC shows the lowest conductivity, only 0.8 S/cm, which is caused by its high porosity and amorphous structure. The CB220 and CB660 carbons show similar conductivities that are both higher than that for AC. The effect of electrical conductivity of carbon on the DCFC performance will be addressed in section 3.6.2.

3.3. Textural Properties of Carbon Fuels. The nitrogen adsorption isotherms of four carbon fuels are shown in Figure 3. The AC shows a type I isotherm characterized by a plateau that is nearly horizontal to the P/P_0 axis. Almost 85% of the pore volume is filled below $P/P_0 = 0.1$, indicating the AC is highly microporous. However, the appearance of hysteresis loops in the AC isotherms implies the existence of some mesopores. The isotherms of CB220, CB660, and GC appear type IV characteristic, with hysteresis loops starting from the medium relative pressures and closing near $P/P_0 = 1$. Patterns of the hysteresis loops seem to be type H3, which is often associated with slit-shape mesopores. The derived values of BET surface area, total pore volume, surface areas of micropores, and mesopores of all carbon fuels are summarized in Table 2. AC shows the highest BET surface area with dominant micropores. The CB220 and CB660 carbons show significantly lower and comparable surface areas, but with dominant mesopores. GC is nearly a nonporous material.

Figure 4 compares the N_2 adsorption isotherms of activated carbon at different particle sizes. These four activated carbons show nearly the same shapes in their type I isotherms possessing highly microporous structures. As shown in the last four rows of Table 2, the decrease of particle size increases the BET surface area and pore volume of AC, which is mainly caused by the increase of mesopores, while the microporous surface area remains nearly unchanged.

3.4. Chemical Reactivity of Carbon Fuels in Air. Temperature-programmed oxidation (TPO) is an efficient tool to evaluate the relative activity of carbon oxidation. The weight

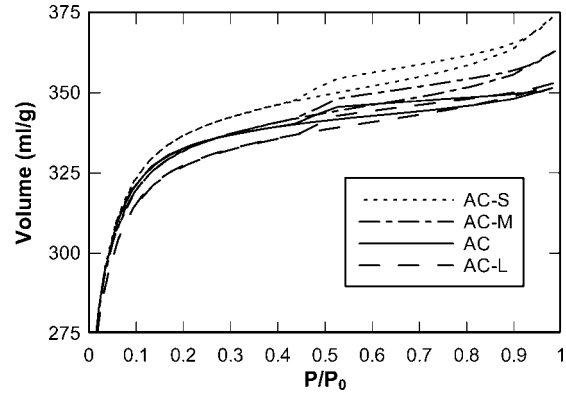

Figure 4. N_2 adsorption isotherms of AC with different particle sizes: AC-S (<0.07 mm), AC-M (0.07−0.25 mm), AC (0.25−0.45 mm), and AC-L (0.45−1.5 mm).

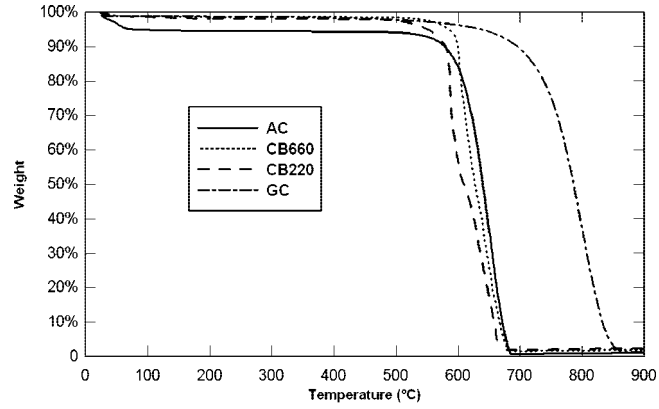

Figure 5. Weight loss curves of AC, CB660, CB220, and GC in TGA tests.

Table 3. XPS Analyses of Surface C and O Concentrations and PZC Values of AC, CB660, CB220, and GC Carbon Fuels

sample	O (%)	C (%)	O/C	PZC
AC	8	90.8	0.088	10.04
CB660	3.4	96.1	0.035	8.31
CB220	1.9	97.9	0.019	8.23
GC	1.1	98.2	0.011	5.28

loss curves of four different carbon fuels are shown in Figure 5. It can be seen that there is a small amount of weight loss below 100 °C for all samples due to the desorption of physisorbed water, and AC exhibits the largest water adsorption capacity due to its significantly higher surface area. The CB220, CB660, and AC carbons have nearly the same thermal stability in the TPO test because their significant weight losses started from 550 °C and ended around 650 °C, which was caused by oxidation of the carbonaceous species. However, the onset weight loss of GC (around 650 °C) was much higher than that of the other carbons. The enhanced thermal stability of GC in air can be attributed to its higher degree of graphitic structure. All of these carbon fuels have an ash content that is less than 2%.

3.5. Surface Oxygen Groups on Carbon Fuels. The atomic concentrations of carbon and oxygen on the carbon surface obtained by XPS are shown in Table 3. The ratio of total oxygen to carbon (O/C) in the topmost atomic layers, which indicates the degrees of surface oxidation of carbon, is also included. As can be seen, the AC has the highest surface oxygen content 8%, while the GC shows the lowest value, only 1.1%. The CB660 and CB220 have moderate surface oxygen amount, 3.4%

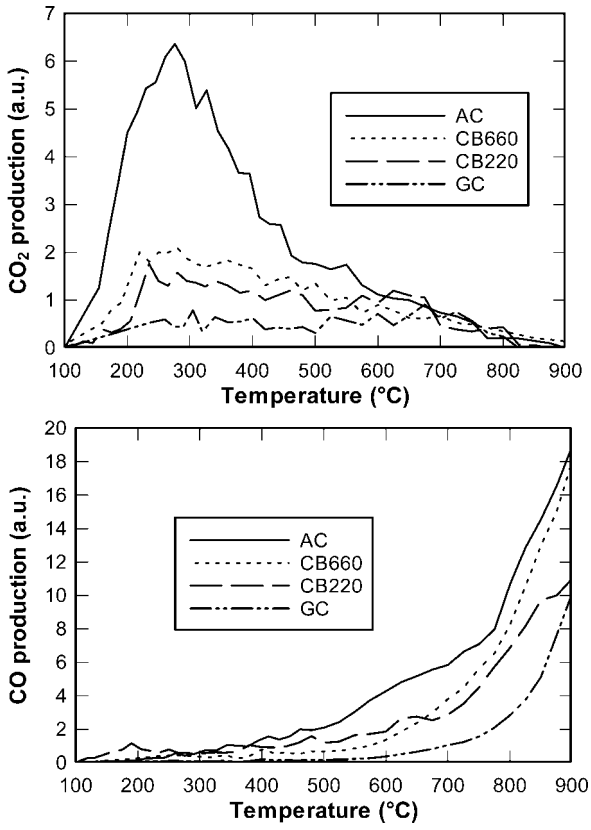

Figure 6. TPD profiles of AC, CB660, CB220, and GC.

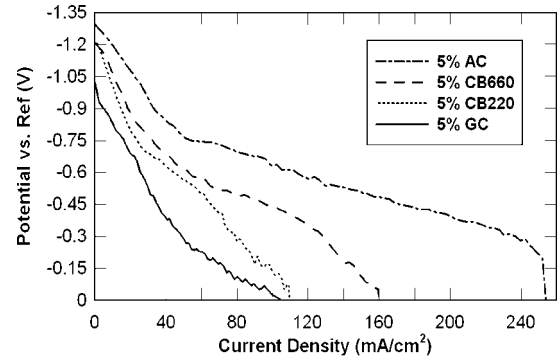

Figure 7. $V-i$ curves of 5% AC, CB660, CB220, and GC at 800 °C with 600 rpm stirring condition.

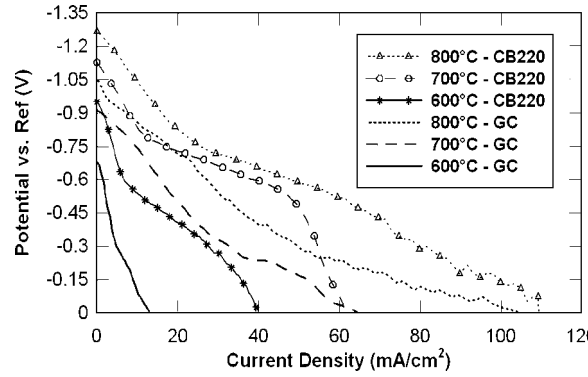

Figure 8. $V-i$ curves of 5% CB220 and GC with 600 rpm at different temperatures.

and 1.9%, respectively. The order of oxygen amount on the carbon surface is as follows: AC > CB660 > CB220 > GC.

The point of zero charge (PZC) value of all carbon fuels was determined by the mass titration method, which provides a good indication about the surface oxygen complexes and the electric surface charges developed by them. This surface charge arises from the interaction between the carbon surface and the aqueous solution and can be used as a convenient index for the surface acidity of carbons.[20,21] As shown in the final column of Table 3, the PZC values decrease in the order of AC > CB660 > CB220 > GC, which is in agreement with the order of surface oxygen complex in XPS tests.

TPD is a commonly used technique to provide the amount, stability, and nature of carbon surface oxygen complex. During the TPD process the surface complexes would release CO_2 and CO at different temperatures. In general, CO_2 evolves from the decomposition of carboxylic acid functionality at low temperatures and/or lactones at high temperatures, while CO arises from the phenols and carbonyls at high temperature.[21] Although it is difficult to directly retrieve information about the exact type of surface functional group, the general information on surface reactive sites can be derived from the TPD profiles.

Figure 6 presents the CO_2 and CO evolution profiles from four different carbon fuels. AC generates by far the largest amount of CO_2 with maximum peak at ca. 270 °C. CB660 and CB220 have lower but comparable evolution amounts for CO_2 with a broad peak at around 200−500 °C with the former producing slightly more CO_2. However, CO_2 by GC is nearly negligible, indicating a surface almost clean of oxygen complex groups. CO evolution took place at a much higher temperature, and there is no obvious CO peak until ca. 500 °C. The order of the CO production is nearly the same as CO_2 production, but the difference of CO productions by different samples is much smaller compared to CO_2 production.

Table 4. Electrochemical Data of AC, CB660, CB220, and GC at Different Temperatures

		AC	CB660	CB220	GC
600 °C, 600 rpm	OCV (V)	−1.04	−0.97	−0.95	−0.68
	i at −0.8 V (mA/cm^2)	13	5	3	
	i at −0.5 V (mA/cm^2)	35	14	12	2.4
	i at −0.2 V (mA/cm^2)	62	41	33	8
	P_{max} (mW/cm^2)	18	11	9	2
700 °C, 600 rpm	OCV (V)	−1.20	−1.15	−1.13	−0.91
	i at −0.8 V (mA/cm^2)	21	18	12	8
	i at −0.5 V (mA/cm^2)	94	52	49	20
	i at −0.2 V (mA/cm^2)	123	80	56	45
	P_{max} (mW/cm^2)	48	27	25	10
800 °C, 600 rpm	OCV (V)	−1.34	−1.25	−1.26	−1.05
	i at −0.8 V (mA/cm^2)	50	37	22	14
	i at −0.5 V (mA/cm^2)	161	86	62	33
	i at −0.2 V (mA/cm^2)	252	137	90	64
	P_{max} (mW/cm^2)	83	46	32	17
G_A of 5% carbon (kJ/mol)		48	101	105	183

3.6. Electrochemical Reactivity of Carbon Fuels in DCFC. 3.6.1. Effect of Carbon Types. Figure 7 shows the anodic polarizations of different carbon fuels with 5% weight loading at 800 °C. The $V-i$ curves of AC, CB220, and CB660 are similar in shape. The curves all drop steeply from OCV to −0.8 V due to the activation resistance, followed by a more stable linear region appearing from −0.8 to −0.3 V, indicating that anodic polarization is under significant ohmic resistance control. Finally, the potential decreases sharply at high current density, which is attributable to concentration polarization. However, the polarization curve of GC shows nearly linear characteristic which implies low electrochemical activity of highly ordered graphitic carbon. Of the four carbon samples, AC always shows the best electrochemical activity which is demonstrated by its most negative OCV and highest current density. In contrast, the GC shows the lowest electrochemical reactivity at different given potentials and different temperatures.

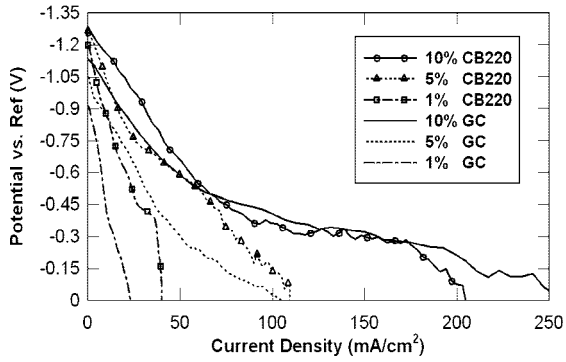

Figure 9. $V-i$ curves of CB220 and GC with 600 rpm at 800 °C with different loadings.

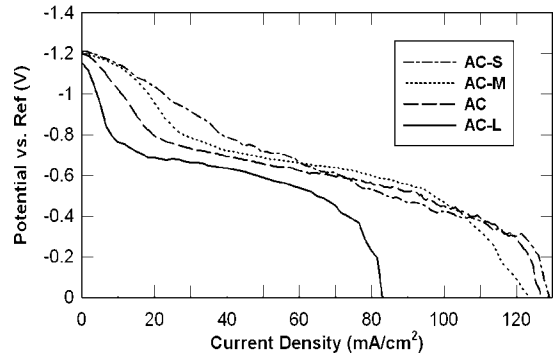

Figure 10. $V-i$ curves of 5% AC-S (<0.07 mm), AC-M (0.07−0.25 mm), AC (0.25−0.45 mm), and AC-L (0.45−1.5 mm) at 700 °C with 600 rpm stirring rates.

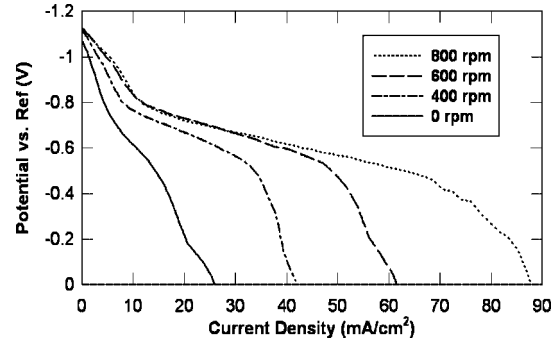

Figure 11. $V-i$ curves of 5% CB220 at 700 °C with different stirring rates.

CB220 and CB660 are nearly equally active, but the latter has a relatively higher discharge rate. In general, the electrochemical reactivities of four carbon fuels increase in such an order: GC < CB220 < CB660 < AC.

In order to study the effect of cell temperature on the electrochemical performance of carbon fuels, the DCFC was tested at 600, 700, and 800 °C, separately, and the quantitative results are listed in Table 4. In Figure 8, we compare the $V-i$ curves of 5% CB220 and 5% GC under the same operational conditions. It can be seen that increasing the cell temperature lifts the OCV to more negative values and substantially increases the current density, particularly from 600 to 700 °C.

The chemical activation energy of carbon fuels can be determined by extrapolation of the apparent activation energy to the OCV according to the following equation:[12,13]

$$G_A' = G_A - \alpha nF(E - E_{eq}) \quad (7)$$

where G_A' is the apparent activation energy at a given potentials, which can be calculated from an Arrhenius plot at three fixed potentials from the $V-i$ curves, G_A is the chemical component of the activation energy, and $\alpha nF(E - E_{eq})$ is the electrochemical component of the activation energy (α is the charge transfer coefficient, n is the number of electrons transferred, F is the Faraday constant, E is the active potential, E_{eq} is the equilibrium potential). The G_A values of four carbon fuels are shown in the last row of Table 4. Although the G_A derived from the $V-i$ curves is a global parameter (including different contributions from activation polarization, ohmic polarization, and concentration polarization), it still reflects the chemical reactivities of carbon fuels in DCFC in the order of GC < CB220 < CB660 < AC.

3.6.2. Effect of Carbon Loading. Figure 9 shows the dependency of $V-i$ curves on the carbon loadings for CB220 and GC. For CB220, 5% and 10% fuel loadings provide nearly the same OCV value, which means that equilibrium OCV value has been reached at 5% CB220 loading. However, GC is a nearly nonporous carbon, much heavier than the other three types of carbons. Consequently, even 10% loading of GC may still not be sufficient to reach the equilibrium OCV. As expected, higher carbon loading always produce higher current density due to the increased contact between carbon and electrolyte.

Interestingly, at 1% and 5% carbon loadings, the CB220 is much more reactive than GC. However, the difference between the $V-i$ curves of two carbon fuels becomes minor when the carbon loading increases to 10%. Especially at lower electrode potentials (−0.25 to 0 V), GC shows a higher current density than CB220. This is caused by the good conductivity of GC, which effectively extends the electrode into the electrolyte and increases the effective surface area of the electrode. Practically, the electrode potential should remain at ca. −0.8 to −0.9 V. We also found that low density carbons such as AC may overflow out of the reactor at high stirring speed. In order to maintain the stable performance of this DCFC, a carbon loading of 5% was chosen in this study.

3.6.3. Effect of Carbon Particle Size. It is known that the particle size of carbon fuels is an important parameter that may affect the anodic discharge rate.[2,4,12] Usually the smaller the carbon particles, the higher the reaction rate in the DCFC. The polarization of 5% AC with different particle sizes at 700 °C are shown in Figure 10. As expected, the AC-L with the largest particle size presents the lowest electrochemical reactivity in these four particle sizes. With the decrease of carbon particle size, the current density increases to higher values at high electrode potentials (from OCV to −0.7 V), which is caused by the larger reactive surface area of finer carbon particles. Whereas, at the low electrode potentials region (from −0.6 to 0 V), AC-S, AC-M, and AC have a comparable current density, which may be due to the insufficient mixing of fine carbon particles with the electrolytes, or the mass transfer resistance cannot be overcome effectively. Practically, the DCFC will operate ca. −0.8 to −0.9 V, instead of over −0.6 V. Therefore, the AC size 0.25−0.45 mm is small enough for comparison.

3.6.4. Effect of Stirring Rate. Figure 11 illustrates the effect of stirring rate on the $V-i$ curves of 5% CB220 operated at 700 °C. It is found that a stirring at 400 rpm can significantly improve the current density compared with the stationary operation due to the improved mass transfer. An increase in stirring rate from 400 to 600 rpm can further improve the current density over the whole electrode potentials range. But a further increase of the stirring rate from 600 to 800 rpm can increase the current density only above ca. −0.65 V, below which the two stirring rates produce nearly the same current density. As

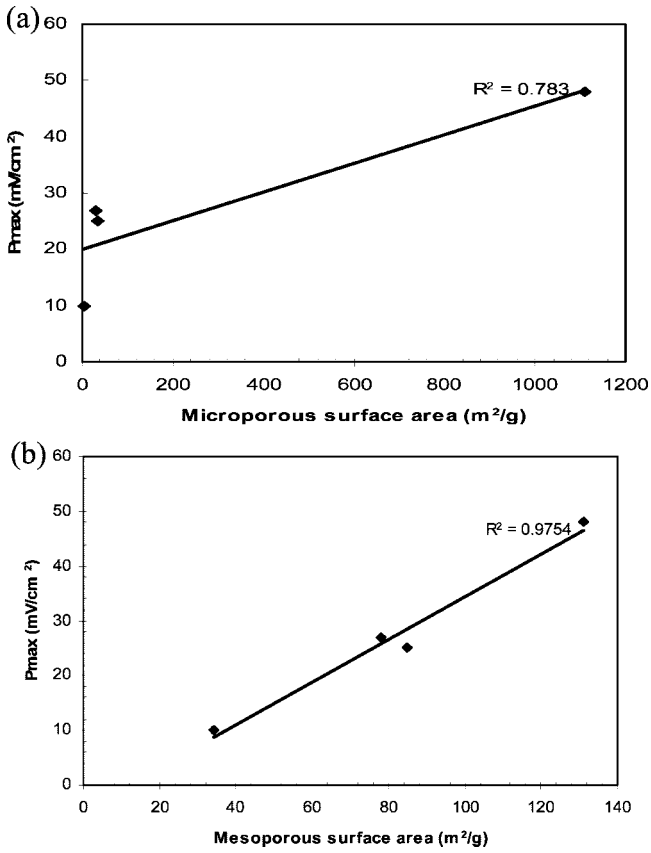

Figure 12. (a) Relationship between P_{max} at 700 °C and microporous surface areas of carbons. (b) Relationship between P_{max} at 700 °C and mesoporous surface areas of carbons.

mentioned above, the practical operational electrode potential would be ca. −0.8 to −0.9 V, and the 600 rpm stirring rate is sufficient for comparing the electrochemical performances of the carbons in the activation resistance control region. A stirring rate of 800 rpm can induce a splashing of the carbon fuel and electrolyte out of the crucible reactor. In general, the 600 rpm stirring rate was found to be the most stable operational condition for our DCFC.

4. Discussion

The experimental results showed that the order of the electrochemical activities of the four selected carbons in DCFC is AC > CB660 > CB220 > GC. An important question arises: what are the key factors affecting the activities of carbon fuels in DCFC? AC has by far the largest surface area and pore volume with dominant micropores, as shown in Figure 3, while GC has the lowest surface area and pore volume. This suggests that a high surface area or pore volume, which can improve the anodic reaction as shown in eq 1 by increasing the contact between carbon fuels and CO_3^{2-}, would be useful for the performance of carbon fuels in DCFC.

The maximum theoretical power density values (P_{max}) are also listed in Table 4. One can see that the total surface area of AC is 10 times that of CB660, but the former has a P_{max} value just ca. 1.6−1.8 times that of the latter at the same temperature, as shown in Tables 2 and 4. The reason is that the dominant micropores of AC are not fully accessible to the molten carbonate electrolyte, and mesopores provide more efficient electrolyte transfer. This is supported by Figure 12a,b, which show that P_{max} at 700 °C increases almost linearly with the carbon mesoporous surface area instead of microporous surface area.

However, CB220 has a higher total and mesoporous surface areas than CB660, but the latter has a higher electrochemical activity than the former (Figure 7). Interestingly, as shown in Figure 6, the order of the CO_2-yielding surface functional groups of the carbons is the same as the order of the activities of the carbons in DCFC, and the CO-yielding functional groups follow the same order. This means that the surface oxygen-containing groups of a carbon also play a key role in regulating the performance of the DCFC. The importance of the surface oxygen groups is consistent with the proposed reaction mechanism in the DCFC,[2,3] which includes several elementary reaction steps:

$$2CO_3^{2-} \rightarrow 2CO_2 + 2O^{2-}$$

$$C_{RS} + O^{2-} \rightarrow C_{RS}O^{2-} \quad \text{first adsorption}$$

$$C_{RS}O^{2-} \rightarrow C_{RS}O^{-} + e^{-} \quad \text{fast discharge}$$

$$C_{RS}O^{-} \rightarrow C_{RS}O + e^{-} \quad \text{fast discharge}$$

$$C_{RS}O + O^{2-} \rightarrow C_{RS}O_2^{2-} \quad \text{slow adsorption (rate-determining step)}$$

$$C_{RS}O_2^{2-} \rightarrow C_{RS}O_2^{-} + e^{-} \quad \text{fast discharge}$$

$$C_{RS}O_2^{2-} \rightarrow CO_2(g) + e^{-} \quad \text{fast discharge and evolution}$$

where C_{RS} is a reactive site on the carbon fuel surface. Apparently, more CO_2- or CO-yielding functional groups provide a highere degree of reactive sites, making the carbon fuels more active in the DCFC.

This is also consistent with the fact that AC, AC-M, and AC-S have different mesoporous surface areas, as shown in Table 2, but their electrochemical activities (Figure 10) are nearly the same. The reason is that they are from the same original carbon AC-L thus with the same surface chemistry.

A higher electrical conductivity of the carbon fuel, which is related to the degree of graphitic structure in the carbon, may be beneficial to the reactivity of the carbon, but this appears not a key issue. GC has the higher conductivity but the lowest reactivity in the DCFC. The reason for this behavior may be that carbon/electrolyte mixture possess sufficient electrical conductivity in the molten situation, and the major reason for the low activity of GC is its highly ordered structure.

5. Conclusions

Four commercial carbon fuels were investigated in our DCFC system and evaluated by $V-i$ curves. Activated carbon showed the highest current density, which reached 49 mA/cm^2 at −0.8 V (vs Au/O_2, $2CO_2$) at 800 °C. The electrochemical reactivity of four carbon fuels was in the order of AC > CB660 > CB220 > GC, which broadly aligns with the concentration of oxygen-containing functional groups on the surfaces of the carbon fuels. A higher operation temperature can improve the carbon anodic performance at 600−800 °C. Increasing the carbon fuel concentration can improve the anodic reactivity, especially for GC as the carbon fuel since a higher concentration can also benefit the charge transport. Moreover, decreasing the particle size in carbon fuels can promote the reactivity to some extent. Anodic reaction rates can be significantly boosted by effective stirring (usually more than 400 rpm) due to minimization of concentration resistance. A carbon with high mesoporous surface area as well as rich surface oxygen-containing groups is desirable fuel for DCFC.

Acknowledgment

Financial support from ARC (Australian Research Council) discovery grant is appreciated.

Literature Cited

(1) Cao, D.; Sun, Y.; Wang, G. Direct carbon fuel cell: Fundamentals and recent developments. *J. Power Sources* **2007**, *167* (2), 250.

(2) Cherepy, N. J.; Krueger, R.; Fiet, K. J.; Jankowski, A. F.; Cooper, J. F. Direct Conversion of Carbon Fuels in a Molten Carbonate Fuel Cell. *J. Electrochem. Soc.* **2005**, *152* (1), A80.

(3) Cooper J. F. Direct conversion of coal and coal-derived carbon in fuel cells. Fuel Cell Science, Engineering and Technology, the International Conference on Fuel Cell Science, Engineering and Technology, 2nd, Rochester, NY, June 14−16, 2004, pp 375−85.

(4) Cooper J. F.; Cherepy N. Carbon fuel particles used in direct carbon conversion fuel cells. US Patent 845939, 2004.

(5) Cooper J. F.; Krueger R.; Cherepy N. A high temperature, molten electrolyte electrochemical cell comprising ash-free turbostratic carbon particles. US Patent 970283, 2001.

(6) Hemmes K.; Cassir M. A theoretical study of the carbon/carbonate/hydroxide (electro-) chemical system in a direct carbon fuel cell. Fuel Cell Science, Engineering and Technology, the International Conference on Fuel Cell Science, Engineering and Technology, 2nd, Rochester, NY, June 14−16, 2004, pp 395−400.

(7) Zecevic, S.; Patton, E. M.; Parhami, P. Direct electrochemical power generation from carbon in fuel cells with molten hydroxide electrolyte. *Chem. Eng. Commun.* **2005**, *192* (10−12), 1655.

(8) Dubois, J.; Millet, J.; Palous, S. Electrochemical oxidation of different modifications of carbon in molten alkaline carbonates. *Electrochim. Acta* **1967**, *12* (3), 241–4.

(9) Hauser V. A study of carbon anode polarization in fused carbonate fuel cells. Corvallis, OR, Oregon State University, PhD Thesis, 1964.

(10) Peelen, W. H. A.; Olivry, M.; Au, S. F.; Fehribach, J. D.; Hemmes, K. Electrochemical oxidation of carbon in a 62/38 mol% Li/K carbonate melt. *J. Appl. Electrochem.* **2000**, *30* (12), 1389.

(11) Vutetakis, D. G. Electrochemical oxidation of carbonaceous materials dispersed in molten carbonate, Columbus, OH, Ohio State University, 1985.

(12) Vutetakis, D. G.; Skidmore, D. R.; Byker, H. J. Electrochemical oxidation of molten carbonate-coal slurries. *J. Electrochem. Soc.* **1987**, *134* (12), 3027.

(13) Weaver R. D.; Leach S. C.; Nanis L. Electrolyte management for the coal air fuel cell. Proceedings of the Intersociety Energy Conversion Engineering Conference, 1981, 16th (Vol. 1), pp 717−21.

(14) Hackett, G. A.; Zondlo, J. W.; Svensson, R. Evaluation of carbon materials for use in a direct carbon fuel cell. *J. Power Sources* **2007**, *168* (1), 111.

(15) Nunoura, T.; Dowaki, K.; Fushimi, C.; Allen, S.; Meszaros, E.; Antal, M. J. Performance of a first-generation, aqueous-alkaline biocarbon fuel cell. *Ind. Eng. Chem. Res.* **2007**, *46* (3), 734.

(16) Pesavento P. V. Carbon-air fuel cell. US Patent 6200697, 2001.

(17) Zecevic, S.; Patton, E. M.; Parhami, P. Carbon-air fuel cell without a reforming process. *Carbon* **2004**, *42* (10), 1983.

(18) Gur, T. M.; Huggins, R. A. High temperature oxygen transport and electrochemical behavior of yttrium barium copper oxide. *J. Electrochem. Soc.* **1993**, *140* (7), 1990.

(19) Pointon, K.; Lakeman, B.; Irvine, J.; Bradley, J.; Jain, S. The development of a carbon-air semi fuel cell. *J. Power Sources* **2006**, *162* (2), 750–6.

(20) Noh, J. S.; Schwarz, J. A. Effect of nitric acid treatment on the surface acidity of activated carbons. *Carbon* **1990**, *28* (5), 675.

(21) Zhu, Z. H.; Radovic, L. R.; Lu, G. Q. Effects of acid treatments of carbon on N_2O and NO reduction by carbon-supported copper catalysts. *Carbon* **2000**, *38* (3), 451.

Received for review June 6, 2008
Revised manuscript received September 30, 2008
Accepted October 6, 2008

IE800891M